Tunneling and revival of Anderson localization in a Bose-Einstein condensate

Sriganapathy Raghav ⬤, Barun Halder, Pradosh Basu, and Utpal Roy ⬤*

Indian Institute of Technology Patna, Bihta, Patna 801103, India

We provide an analytical model to fabricate an exponential localization of a Bose-Einstein condensate under a bichromatic optical lattice. Such localization is famously known as Anderson localization. The degree of localization is investigated using the participation ratio to recognize the laser parameter domain for Anderson localization. The exponential nature of the localization is proved, and we also identify the localization length. The tunneling of an Anderson-localized condensate with time is observed, and the revival phenomenon of Anderson localization is reported. Slowing down of Anderson localization is noticed for higher laser intensity. We also study the dynamical and structural stability of the condensate during Anderson localization, which suggests the preferred values of laser power and the time instance to encounter a minimal mean difference in the presence of noise.

I. INTRODUCTION

In 1958, Anderson demonstrated exponential localization when the on-site energies of the lattice were randomly shuffled [1]. Since then, there has been an extensive search for ways in condensed-matter systems to manifest exponentially localized wave functions in spatial coordinates [2–5]. However, the condensed-matter system did not turn out to be a favorable candidate, and scientists also started looking for possibilities in ultracold atoms. Billy *et al.* were the first to report exponential localization in ultracold matter waves [6], followed by various other groups [7–11]. In recent work, Sbroscia *et al.* observed Anderson localization for a two-dimensional quasicrystalline optical lattice [12]. The study of ultracold atoms in quasicrystalline optical lattices like the bichromatic optical lattice (BOL) has become the center of attention for quantum simulation research [13–16]. When two optical lattices of different wavelengths and depths overlap, one may obtain a geometrically frustrated potential BOL [17]. A variety of interesting physics have emerged using ultracold atoms trapped in a BOL potential [18–23]. There are numerous theoretical studies about ultracold atoms in BOLs utilizing the Bose-Hubbard model and numerical solutions of the Gross-Pitaevskii equation (GPE) [24–28]. Adhikari and Salasnich carried out numerical studies on the localization of Bose-Einstein condensate (BECs) in BOLs of one, two, and three dimensions with different nonlinearities [29]. The exact analytical model for BECs inside a BOL was reported by Nath *et al.* [30,31], who studied the solutions for both attractive and repulsive nonlinearities with precise trap engineering.

Anderson localization in BECs is thought of as a highly localized condensate cloud of an exponentially varying profile that is formed inside a disordered potential like a BOL with periodic lattice frustrations. However, Anderson localization happens only in the frustrated lattice sites instead of other potential minima for a highly intense BOL trap. Identifying a precise parameter regime of Anderson localization is definitely a matter of concern in experiments. A natural question is whether this sharply localized cloud in the frustrated site can be transported to the other frustrated sites by overcoming the high potential barrier of the intense BOL. Second, during transportation, if any, additional questions include what the temporal dynamics of the Anderson-localized condensate might be and whether such localization disappears forever after tunneling.

In this work, we address all these issues with an exact analytical, time-dependent model for BECs under a BOL potential. We prove the exponential localization through an analytical approach and predict the localization length for BECs. The trap engineering of such localization is also reported for experimental feasibility. The parameter regime of Anderson localization is demarcated by the nature of the participation ratio (PR). Tunneling of such an Anderson-localized cloud is studied for the condensate in the presence of an initial drift [32–34]. The nature of the tunneling is illustrated by time snapshots of condensate density and the rise or decay of localization inside the frustrated site. The periodic occurrence of Anderson localization with time is observed and reported as the revivals of such localization during tunneling. Moreover, we demonstrate the variation of the revival time with a tunable BOL parameter and deceleration of the exponentially localized cloud. The numerical stability of the exponentially localized condensate is studied at different times, establishing the present model as a sufficiently stable configuration.

II. ANALYTICAL MODEL FOR LOCALIZATION

The dynamics of BECs are analytically modeled using the GPE, a modified form of Schrödinger's equation with a nonlinearity term [35,36]. The nonlinearity can be controlled by modulating the atomic scattering length using the Feshbach

*uroy@iitp.ac.in

resonance technique. The exact analytical model for BECs has been obtained for various external traps, including harmonic, double well, periodic, and quasiperiodic [37–40]. The present work focuses on obtaining the time-varying solution to the one-dimensional (1D) GPE for a stationary BOL and studying the transport of Anderson localization. We obtain solutions that cover a wide range of situations, such as periodic or localized, based on modulus parameters of the elliptic function. The bright or dark solitary excitations are obtained based on interatomic interactions, and we study how they propagate across the lattice. To build the exact analytical model, we start with a dimensionless 1D GPE of weakly interacting ultracold atoms with cubic nonlinearity:

$$i\frac{\partial \psi(z,t)}{\partial t} + \frac{1}{2}\frac{\partial^2 \psi(z,t)}{\partial z^2} - g(z,t)|\psi(z,t)|^2 \psi(z,t)$$
$$- V(z)\psi(z,t) - i\tau(z,t)\psi(z,t) = 0. \tag{1}$$

Here, $\psi(z,t)$ is the 1D condensate wave function, $g(z,t)$ denotes the space- and time-modulated nonlinearity, and $\tau(z,t)$ represents the space- and time-modulated loss or gain of the condensate atoms. For the purpose of illustration, we have exploited experimentally feasible parameters of ^{7}Li BECs trapped in a 1D waveguide of transverse frequency $\omega_\perp = 2\pi \times 710$ Hz, optical lattice wavelength $\lambda = 10.62$ μm, and s-wave scattering length $a_s = -0.21$ nm, and the harmonic oscillator length in the transverse direction is $a_\perp = \sqrt{\frac{\hbar}{M\omega_\perp}} = 1.4245$ μm [41]. The dynamics of the condensate can efficiently be controlled by the axial external trap $V(z)$, which can be engineered by varying the applied magnetic field and the angle between the overlapping laser beams [42]. To obtain an Anderson localization, we require a BOL, which possesses frustrated potential sites. A BOL potential is created by the application of two laser beams of different wavelengths and different powers. The potential under consideration is given by

$$V(z) = V_1 \cos(2lz) + V_2 \cos(lz). \tag{2}$$

The potential depths V_1 and V_2 are related to the recoil energy of the constituent lasers of wavelength λ. The exact spatially localized solution of the variable coefficient nonlinear Schrödinger equation [Eq. (1)] is nontrivial in the presence of a trap, and thus, we perform a similarity transformation, which connects it to a known solvable nonlinear equation with constant coefficients, leaving behind a set of consistency conditions. The corresponding ansatz is written as

$$\psi(z,t) = A(z,t)F[Z(z-vt)]e^{i\theta(z,t)}, \tag{3}$$

such that the traveling coordinate is taken in a simple form: $Z(z-vt) = B(z) + D(t)$. Here, v is a uniform speed, which can be associated with experimental situations where the BEC is moved horizontally, either by coherently moving the lattice [32] or by imparting momentum using a pulsed standing-wave laser field [33,34]. The condensate density $F[Z(z-vt)]$ and the phase $\theta(z,t)$ are expected to depend on the trap parameters of the external BOL potential and initial velocity of the cloud. The real part of the equation, upon substituting the above ansatz with traveling coordinates,

becomes

$$-A(z,t)F[Z(z-vt)]\theta(z,t)_t + \frac{1}{2}A_{zz}(z,t)F[Z(z-vt)]$$
$$+ A(z,t)_z \frac{\partial F[Z(z-vt)]}{\partial Z(z-vt)}\frac{\partial Z(z-vt)}{\partial z}$$
$$+ \frac{1}{2}A(z,t)\frac{\partial^2 F[Z(z-vt)]}{\partial Z(z-vt)^2}\left(\frac{\partial Z(z-vt)}{\partial z}\right)^2$$
$$+ \frac{1}{2}A(z,t)\frac{\partial F[Z(z-vt)]}{\partial Z(z-vt)}\frac{\partial^2 Z(z-vt)}{\partial z^2}$$
$$- \frac{1}{2}A(z,t)F[Z(z-vt)]\theta(z,t)_z^2$$
$$- g(z,t)A(z,t)^3 F[Z(z-vt)]^3$$
$$- V(z)A(z,t)F[Z(z-vt)] = 0. \tag{4}$$

The subscript variables imply partial differentiation. To explore the connection between the trap parameters and the nonlinearity, we mapped the dynamics with the following known nonlinear differential equation, which also helps us find the proper consistency conditions:

$$\frac{\partial^2 F[Z(z-vt)]}{\partial Z(z-vt)^2} - GF[Z(z-vt)]^3 = 0, \tag{5}$$

where the constant $G = 2g(z,t)A^2(z,t)/Z_z^2(z,t)$ is the nonlinearity constant. G is -1 for attractive interatomic interactions and 1 for repulsive ones. This nonlinear equation is taken in the form of the elliptic equation, which is known to manifest solitary-wave excitations [43]. The elliptic equation has 12 solutions as Jacobi elliptic functions, among which $cn[Z(z-vt),m]$ and $sn[Z(z-vt),m]$ are widely used. The modulus parameter m controls the nature of excitations, such that $m = 0$ manifests a periodic solution, $0 \leqslant m \leqslant 1$ produces cnoidal waves, and $m = 1$ manifests a localized solution. The latter is the case under consideration. After connecting Eq. (5) with the elliptic equation, the real part is left with the following consistency conditions, relating the amplitude, phase, and spatial part of the traveling coordinate:

$$\frac{A_{zz}(z,t)}{2A(z,t)} - \theta_t(z,t) - \frac{\theta_z(z,t)^2}{2} - V(z) = 0, \tag{6}$$

$$[A^2(z,t)B_z(z)]_z = 0. \tag{7}$$

We carry out a similar calculation for the following imaginary part of Eq. (1) after the substitution of the ansatz with the traveling coordinate:

$$A_t(z,t)F[Z(z-vt)] + A(z,t)\frac{\partial F[Z(z-vt)]}{\partial Z(z-vt)}\frac{\partial Z(z-vt)}{\partial t}$$
$$+ A(z,t)_z F[Z(z-vt)]\theta_z(z,t)$$
$$+ A(z,t)\frac{\partial F[Z(z-vt)]}{\partial Z(z-vt)}\frac{\partial Z(z-vt)}{\partial z}\theta_z(z,t)$$
$$+ \frac{1}{2}A(z,t)F[Z(z-vt)]\theta_{zz}(z,t)$$
$$- \tau(z,t)A(z,t)F[Z(z-vt)] = 0, \tag{8}$$

which brings out another set of consistency equations:

$$D_t(t) + B_z(z)\theta_z(z,t) = 0, \qquad (9)$$

$$2A(z,t)A_t(z,t) + [A^2(z,t)\theta_z(z,t)]_z - 2\tau(z,t)A^2(z,t) = 0. \qquad (10)$$

The consistency equations are carefully solved to obtain the following solutions, subject to the substitution of the form of the BOL trap:

$$D(t) = -vt + a_1, \quad \theta_z(z,t) = \frac{v}{B_z(z)}, \quad A^2(z,t) = \frac{c(t)}{B_z(z)},$$

$$g(z,t) = GB_z^2(z)/2A^2(z,t), \quad \tau(z,t) = \frac{1}{2}\frac{c_t(t)}{c(t)}. \qquad (11)$$

Here, a_1 signifies the center-of-mass position of the condensate at the initial time, and $c(t)$ is an arbitrary positive-definite function of time, which is taken as a constant, $c(t) = c$, in our illustration to account for zero loss or gain, i.e., $\tau(z,t) = 0$. The above equations have a direct dependence of phase and nonlinearity on the spatial derivative of the traveling coordinate $B_z(z)$ of the system, which will be decided by the external trap. We aim to find the exact form of the traveling coordinate $Z(z - vt)$ to find the explicit expression for all the related physical parameters by simplifying the above expressions along with Eq. (6). We arrive at the expression for the spatial function of the traveling coordinate $B(z)$, which helps us write the traveling coordinate as

$$Z(z - vt) = \gamma e^{a_2} \int_0^z e^{\beta\cos(lz')}dz' - vt + a_1, \qquad (12)$$

where the first term is the function $B(z)$ and a_1 and a_2 are constants of integration. The phase of the wave function is obtained by combining the coordinates of Eqs. (6) and (9) by using the form of $B(z)$ and $D(t)$:

$$\theta(z,t) = \frac{v}{\gamma}e^{-a_2}\int_0^z e^{-\beta\cos(lz')}dz' + \frac{\beta^2 l^2}{16}t + a_3. \qquad (13)$$

Here, a_3 is an integration constant signifying an initial phase at the origin if there is any. One can also write the amplitude $A(z,t)$ and the nonlinearity $g(z,t)$ by substituting the evaluated expression of $B(z)$. The most crucial expression as far as the experimental utility is concerned is for the physical parameters of the constituent lasers forming the BOL, and we obtain the potential parameters as

$$V_1 = \frac{-\beta^2 l^2}{16}, \quad V_2 = \frac{\beta l^2}{4}. \qquad (14)$$

These equations suggest that any arbitrary potential parameters may not support exciting solitary waves in BECs. Our analytical model contributes to that issue by identifying the
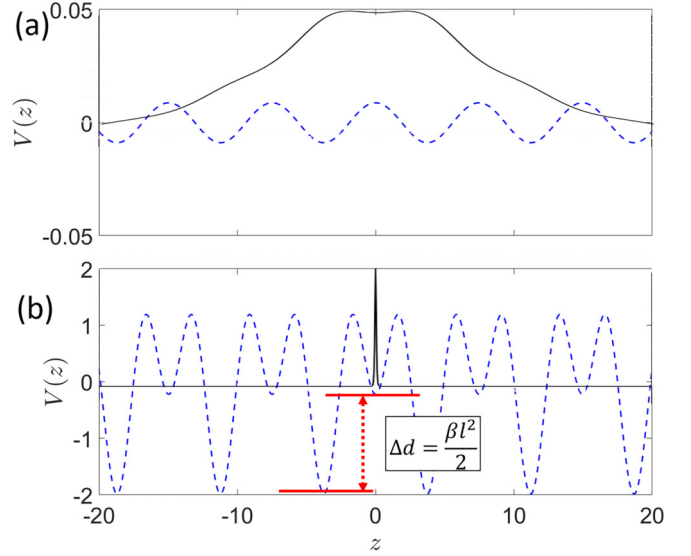

FIG. 1. The potential profile (dotted lines) of BOL for various potential parameters: (a) $\beta = 0.05$ and (b) $\beta = 5$. Solid lines represent condensate density. z is scaled by harmonic oscillator length $a_\perp = 1.4245$ μm, and $V(z)$ is scaled by $\hbar\omega_\perp$, where $\omega_\perp = 2\pi \times 710$ Hz.

parameter related to obtaining a solitary wave that can manifest Anderson localization. In fact, the ratio between the laser amplitudes $\frac{V_1}{V_2}$ is obtained as $\frac{\beta}{4}$. Hence, β controls the shape of the potential by relative changes in the laser amplitudes. This helps to manufacture an appropriate trap to investigate a variety of solitary excitations. We depict the potential profiles in Fig. 1 to show the preparation of the trap for Anderson localization with higher β for a given l. The geometrical lattice frustration appears and becomes dominant for larger β. The difference between the lattice depth and frustrated depth is $\Delta d = \frac{\beta l^2}{2}$, which is responsible for the localization at higher β values, as delineated by the condensate density in Fig. 1(b). This depth difference, which is responsible for localization, is similar to the depth difference in the tight-binding model originally considered by Anderson for electronic systems [1]. To analytically establish such localization, we evaluate all the functions required to express a time-dependent wave function of the condensate under a BOL trap. It is well known that attractive interatomic interaction manifests bright solitary waves, whereas repulsive interaction supports dark solitary waves [29,36,44,45]. It was already mentioned that a nonlinear Schrödinger equation possesses solutions in the form of Jacobian elliptic functions: $cn[Z(z - vt), m]$ and $sn[Z(z - vt), m]$ for attractive and repulsive interactions, respectively. Accordingly, we can write the final form of the wave functions with appropriate elliptic functions:

$$\psi(z,t) = \sqrt{\frac{c(t)}{\gamma e^{\beta\cos(lz)}}}\, cn\left[\left(\gamma e^{a_2}\int_0^z e^{\beta\cos(lz')}dz' - vt + a_1\right), m\right]e^{i\theta(z,t)}, \qquad (15)$$

$$\psi(z,t) = \sqrt{\frac{c(t)}{\gamma e^{\beta\cos(lz)}}}\, sn\left[\left(\gamma e^{a_2}\int_0^z e^{\beta\cos(lz')}dz' - vt + a_1\right), m\right]e^{i\theta(z,t)}, \qquad (16)$$

TABLE I. Critical number of atoms at two scattering lengths for a set of aspect ratios of longitudinal and transverse trap frequencies and their corresponding K values. The values of γ and c are taken to be 0.1 and 10^4, respectively.

$\Lambda = \frac{\omega_z}{\omega_\perp}$	$K = \frac{N_c\|a_{s,\max}\|}{a_\perp}$	N_c for $\|a_{s,\max}\| = 0.21$ nm	N_c for $\|a_{s,\max}\| = 0.15$ nm
0.1	0.460	3120	4370
0.5	0.560	3800	5320

where the expression of $\theta(z, t)$ is given in Eq. (13). The first equation is for an attractive regime, and the latter represents repulsive interaction. In both cases, a family of solutions is found for various modulus parameters m. In the present work, we are interested in the localization of the condensate and consider the solution with $cn[Z(z - vt), m = 1] = \mathrm{sech}Z(z - vt)$ for further investigation.

It is also well known that bright excitations under attractive interaction are stable up to a certain critical number of atoms N_c [41,46–51]. This critical number of atoms is evaluated by comparing the nonlinearity obtained in Eq. (11) and the general relation of nonlinearity with the space-distributed scattering length [52]. Some obtained critical numbers are tabulated in Table I. Two different scattering lengths are considered with their maximum values to obtain the limit. The trap asymmetry Λ and K values are crucial for evaluating N_c. The obtained nonlinearity in our model is space distributed, and also $g(z) = \sqrt{2\pi \Lambda N_c a_s(z)}/a_\perp$. The nonlinearity attains its maximum value in the vicinity of Anderson localization, which can be further reduced to increase the critical number of atoms. The experimental viability of our model will rely on these critical numbers.

III. IDENTIFYING THE PARAMETER REGIME OF LOCALIZATION THROUGH THE PARTICIPATION RATIO

We are interested in the dynamics of Anderson localization, which should occur for attractive interactions. However, the solution covers various situations corresponding to the potential parameters, β and, l, associated with the power and wavelength of the laser. For a given wavelength of the laser, we investigate the condensate cloud for various β to identify the region of localization. The degree of localization is understood in terms of the PR [53], which is defined in terms of the obtained wave function as [54]

$$\mathrm{PR} = \frac{1}{\int_{-\infty}^{\infty} |\psi(z, t)|^4 dz}. \tag{17}$$

Physically, PR measures the number of lattice sites over which the wave function is extended. A PR value of 1 denotes that the wave function extends over all the lattice sites, and a PR closer to zero denotes single-site participation. Figure 2 shows how PR changes with increasing laser power. There is a smooth fall of PR for increasing β, and interestingly, one could note a sudden descent towards zero after β reaches 4.16. This is an indication of the emergence of prominent localization from extended states. The value of β at which this transition occurs is denoted by β_c. The insets in Fig. 2 show the condensate densities before, after, and at β_c. It is observed that at $\beta = \beta_c$, the height of the density in the central site is equal to that in neighboring sites. It is important to discuss the change in the behavior of the condensate for lower and higher β with respect to β_c. We have studied these two regimes by fitting them using suitable functions as shown in Eq. (18). And the parameters for the best fit are estimated as follows: $A_1 = 0.154, A_2 = 0.842, A_3 = 0.881, A_4 = 0.166$ for the $\beta < \beta_c$ regime and $B_1 = 0.0086, B_2 = 0.152$,
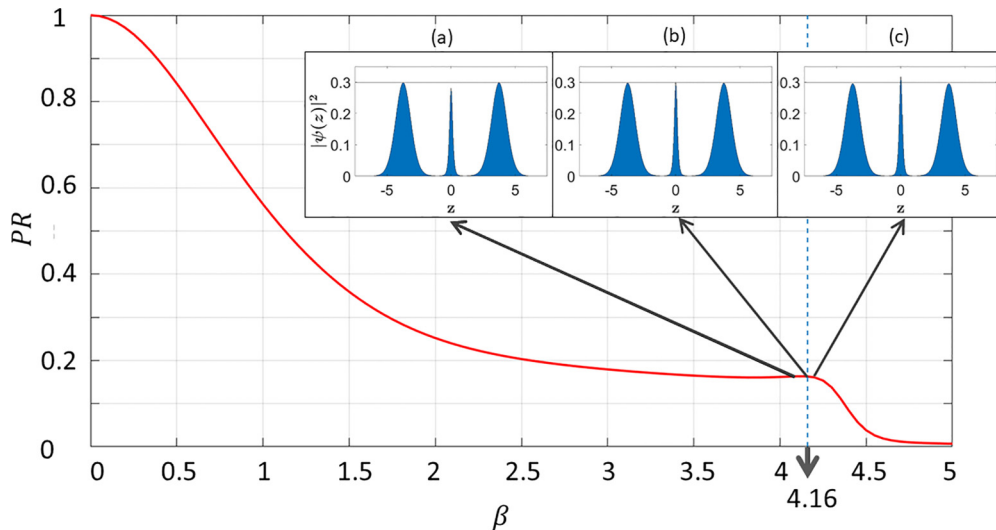

FIG. 2. Participation ratio for different β values. The dashed line indicates $\beta_c = 4.16$, to the right of which is the domain for Anderson localization. The insets show the condensate densities for (a) $\beta = 4.15$, (b) 4.16, and (c) 4.17. Others parameters are given in dimensionless units: $G = -1, t = 0, c = 10^4, l = 0.84$, and $\gamma = 0.1$.
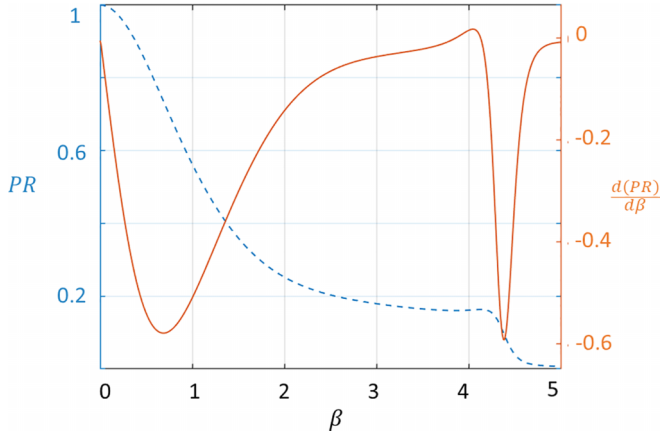
FIG. 3. Participation ratio (dashed line) and its derivative with respect to β (solid line) for various β values. We have used the same parameters as in Fig. 2.

$B_3 = 17.83$ for the $\beta > \beta_c$ regime:

$$\text{PR}_{(\beta < \beta_c)} = A_1 + A_2 e^{-A_3\beta^2 + A_4\beta^3},$$
$$\text{PR}_{(\beta > \beta_c)} = B_1 + B_2 e^{-B_3(\beta - \beta_c)^2}. \tag{18}$$

It is worth observing that, for $\beta < \beta_c$, A_3 dominates over A_4. However, the widths of the Gaussian fit for both regions are quite dissimilar, such that $B_3 \gg A_3$. Hence, we infer that when the laser power is below the critical value ($\beta < \beta_c$), the rate at which the PR saturates is much slower than the rate at which it reaches saturation for $\beta > \beta_c$. The two regimes, $\beta < \beta_c$ and $\beta > \beta_c$, are further understood by computing the slope of PR with respect to β. Figure 3 shows the variation of $\frac{d(PR)}{d\beta}$ with respect to β along with the PR variation (dotted curve). The two minima indicate the constant variation of PR before it reaches saturation in the two regimes. The curves in the $\beta > \beta_c$ regime are much narrower than in the first regime since the rate at which PR saturates is faster in the higher-β regime. The first regime implies localization towards the first two neighboring lattice sites around the origin, $z = 0$. However, this is neither an exponential localization in the central frustrated site nor an Anderson localization. On the other hand, the second domain for $\beta > \beta_c$ manifests a distinct behavior, as shown by the variations of PR and its slope. This emerges due to the localization in the central frustrated site when the frustrated lattice depth is significant compared to the main lattice depth. The transition point between these two domains is identified by the transition of the slope from positive to negative, which happens at $\beta = \beta_c = 4.16$. The minimum of the curve in the second domain corresponds to 50% occupancy of the central frustrated site around $\beta = 4.48$. We will soon prove that the localization of the second domain is an exponential localization and call it Anderson localization.

A. Characterizing the Anderson localization

Before getting into the time-dependent dynamics, explicitly for the Anderson-localized cloud, we need to characterize it in terms of localization length to establish the exponential localization property. In disordered physical systems, it is ob-

TABLE II. The fitting parameters for the exponential localization: a, b, and ζ [Eq. (19)], with corresponding R^2 values. The localization length is scaled by the harmonic oscillator length $a_\perp = 1.4245$ μm.

β	a	b	ζ	R^2
4.2	-0.2021	9.4038	0.1274	0.9979
4.4	-0.1171	12.4731	0.0938	0.9979
4.6	-0.0687	16.7402	0.0707	0.9982
4.8	-0.0401	22.6492	0.0541	0.9987
5	1	31.2252	0.0413	0.9991
5.2	1	42.7321	0.0321	0.9995
5.4	1	58.6585	0.0252	0.9997
5.6	1	80.1018	0.0198	0.9999
5.8	1	107.73	0.0158	0.9999
6	1	141.523	0.0127	0.9999

served that the localization falls exponentially in space as $e^{\frac{-|z|}{\zeta}}$, where ζ is called the Localization length [55]. In our work, we consider the variation of the profile of the condensate cloud with respect to z in the domain, demarcated by $\beta > \beta_c$. The variations are studied for many values of the potential parameter β. In each case, the curve is examined to determine whether it fits exponential nature:

$$a + be^{-\frac{|z|}{\zeta}}. \tag{19}$$

We observe that the variations are indeed consistent with the exponential nature. The localization length is obtained by curve fitting in ζ as per Eq. (19). The parameters for the best fit are estimated and are presented in Table II with corresponding R^2 values. The R^2 values close to 1 indicate the goodness of our fit, confirming the existence of exponential localization or Anderson localization. On the other hand, the exponential function does not become a good fit for the
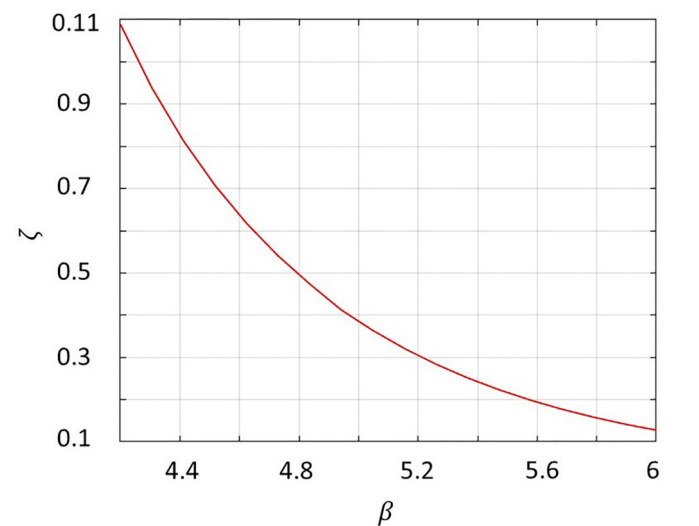

FIG. 4. Variation of the localization length ζ with respect to β in the localization domain, i.e., $\beta > \beta_c$. The other dimensionless parameters are $G = -1$, $t = 0$, $c = 10^4$, $l = 0.84$, and $\gamma = 0.1$. The localization length is scaled by harmonic oscillator length $a_\perp = 1.4245$ μm.
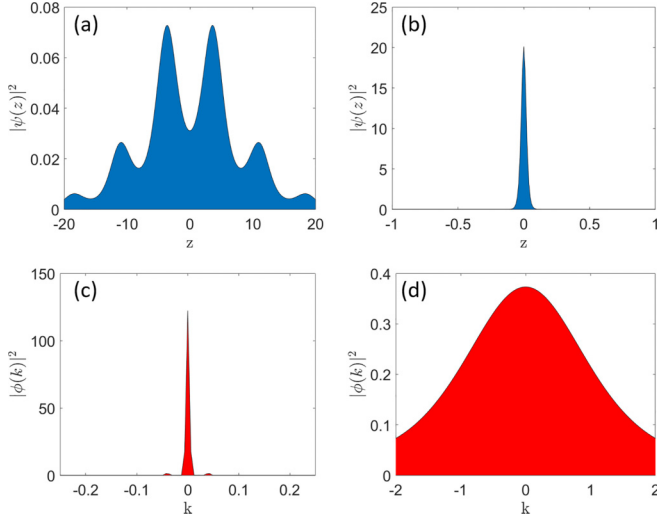
FIG. 5. Condensate density in coordinate space for β values of (a) 0.5 and (b) 6. Condensate density in momentum space for β values of (c) 0.5 and (d) 6. Here, the dimensionless parameters include $G = -1$, $c = 10^4$, $l = 0.84$, $\gamma = 0.1$, and $v = 1$. z is scaled by $a_\perp = 1.4245\,\mu$m, and k is scaled by $a_\perp^{-1}$.

condensate at $\beta < \beta_c$. The parameter ζ in the above fit gives us the localization length, which is obtained for laser powers $\beta > \beta_c$, and the results are shown in Fig. 4. When one tries to control Anderson localization by altering the external trap, it becomes important to know the variation of the localization length with β. The length of localization falls steadily with increasing β, which also follows a regular pattern in the form of an exponential function:

$$\zeta = c_1 + c_2 e^{-c_3 \beta}. \tag{20}$$

The parameters c_1, c_2, and c_3 are evaluated as 0.0048, 38.04, and 1.406, respectively. It is also observed that the localization length tends to saturate at $\zeta = 0.0048$, implying a very sharp density spike for a very large value of β without deviating from the exponential nature of the density profile.

B. Broadening of momentum distribution

The comparison of condensate density in coordinate space with the momentum space gives us more insights into the physics of matter-wave localization. It is expected from the uncertainty principle that the momentum distribution for the localized states must be broadened, indicating the range of momentum carried by the constituent atoms. Figures 5(a) and 5(b) show the condensate density in coordinate space for $\beta = 0.5$ and 6, respectively, and Figs. 5(c) and 5(d) show the condensate density in momentum space for $\beta = 0.5$ and 6, respectively. For low disorders such as $\beta = 0.5$, the BOL resembles an optical lattice with the BEC spread across various lattice sites corresponding to a single momentum peak in reciprocal space. This situation is reversed in higher disorders such as $\beta = 6$, where the condensate is localized to a single site due to the scattering of component waves by frustrated lattice sites.

IV. COLLAPSE AND REVIVALS OF ANDERSON LOCALIZATION

In the previous section, we revealed the parameter domain for Anderson localization and how one can control it by tuning the external trap. Here, we study the tunneling of the Anderson-localized cloud across the BOL sites. The time-dependent density of the condensate is obtained from Eq. (15), which is a function of the traveling coordinate. Hence, knowing the nature of the traveling coordinate is important for analyzing the tunneled cloud at the real position z and time t. Variations of $Z(z - vt)$ in Eq. (12) with the real position coordinate at times $t = 0$ and $t = 13.5$ (in units of $\omega_\perp^{-1}$) are depicted in Figs. 6(a) and 6(b), respectively. Each plot shows two β values, one below β_c (2.5) and another above β_c (4.5). We observe that, for $\beta \to 0$, the traveling coordinate resembles a straight line with slope γ for all times. However, higher β values resemble a staircaselike traveling coordinate. The origin, $z = 0$, does not depend on β but creates an offset in the vertical axis due to the temporal drift of the condensate. In Fig. 7, we closely observe the condensate
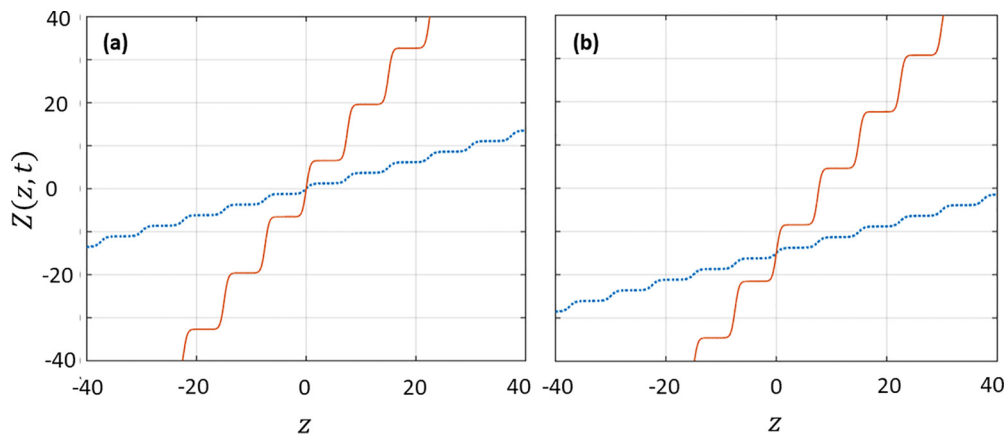

FIG. 6. Variation of the traveling coordinate with respect to z for times (a) $t = 0$ and (b) $t = 13.5$ and β values of 2.5 (dotted line) and 4.5 (solid line). Here, the dimensionless parameters include $G = -1$, $c = 10^4$, $l = 0.84$, $\gamma = 0.1$, and $v = 1$. The constants a_1 and a_2 are taken to be zero for simplicity. z is scaled by harmonic oscillator length $a_\perp = 1.4245\,\mu$m, and t is scaled by the inverse of transverse frequency $\omega_\perp^{-1} = 0.2242$ ms.
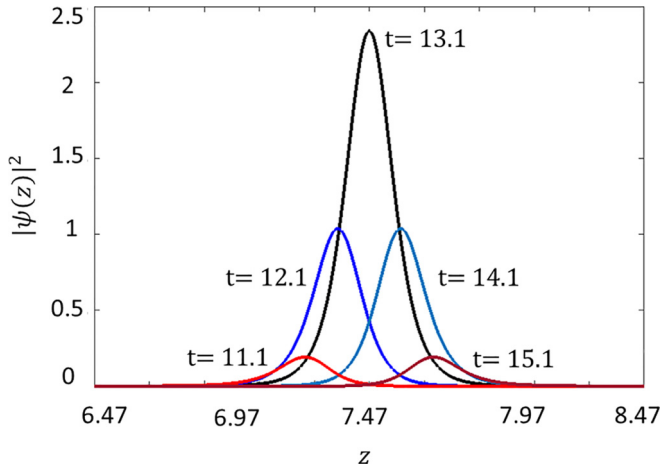
FIG. 7. Time evolution of the Anderson-localized condensate in the frustrated site for $\beta = 4.5$. Here, the dimensionless parameters includes $G = -1$, $c = 10^4$, $l = 0.84$, $v = 1$, and $\gamma = 0.1$. Here, z is scaled by harmonic oscillator length $a_\perp = 1.4245$ μm, and t is scaled by the inverse of the transverse frequency $\omega_\perp^{-1} = 0.2242$ ms. $|\psi(z)|^2$ is in units of $a_\perp^{-1}$.

density at the frustrated site ($z = 7.47a_\perp$) in the domain of Anderson localization ($\beta = 4.5$); we observe a rise and a decay of the localization with a small change in evolution time from $t = 11.1$ to $t = 15.1$ (in units of $\omega_\perp^{-1}$). As we are dealing with a normalized density, the rise and decay of the localization signify that the cloud tunneled in and tunneled out of the frustrated lattice site, respectively. Such tunneling of an Anderson-localized cloud for a highly intense BOL trap (large β) seems interesting and encourages us to study the cloud postdecay with time.

A. The revival dynamics of Anderson localization

The rise and decay of the Anderson-localized condensate in the frustrated site is a clear signature of quantum-mechanical tunneling across the lattice sites. However, Anderson localization happens at the frustrated lattice sites, which appear in spatially periodic intervals in a BOL trap. As each frustrated site is surrounded by two main lattice sites, the immediate tunneling of the density will happen to the neighboring lattice site instead of a frustrated one. In Fig. 8, we show the time evolution of Anderson-like localization for $\beta = 4.5$ and $l = 0.84$. The nature of tunneling remains the same even for a very high value of β, where the condensate is just a sharp spike. Various density snapshots are shown at different times, $t = 0, 6.55, 13.1, 19.65$, and 26.2, in units of $\omega_\perp^{-1}$. One can observe that the Anderson localization in the frustrated lattice site revives after every $13.1\omega_\perp^{-1}$, and the density becomes a replica of the initial Anderson-localized condensate. This time is designated as the revival time t_R of Anderson localization. During the half integrals of the revival time (i.e., $t = t_R/2, 3t_R/2, \dots$), we can see an intermediate accumulation of the condensate density at the main lattice sites. Therefore, the Anderson-localized cloud not only tunnels across the lattice sites but also reappears at the next frustrated site after a time t_R. In general, the reoccurrence times are $t = nt_R$ for $n = 0, \pm 1, \pm 2, \pm 3, \dots,$
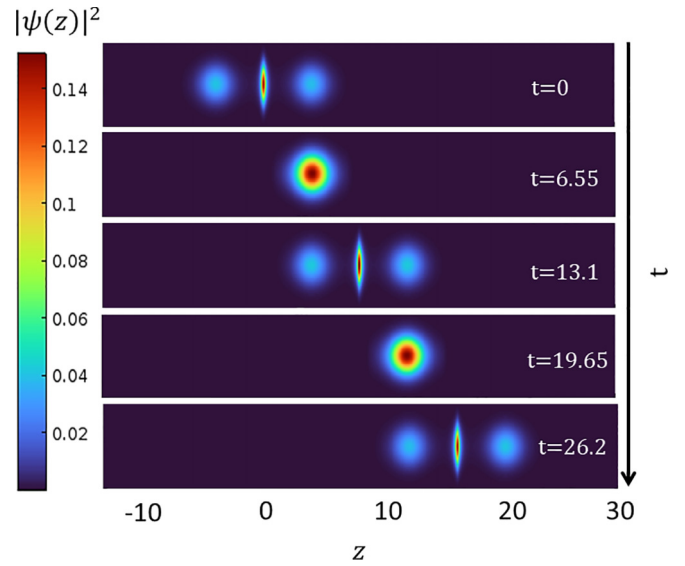

FIG. 8. Snapshots of the condensate density with $\beta = 4.5$ at specific times: 0, $t_R/2$, t_R, $3t_R/2$, and $2t_R$, where $t_R = 13.1$. The dimensionless parameters are $G = -1$, $c = 10^4$, $l = 0.84$, $v = 1$, and $\gamma = 0.1$. Here, z and t are scaled by harmonic oscillator length $a_\perp = 1.4245$ μm and the inverse of transverse frequency $\omega_\perp^{-1} = 0.2242$ ms, respectively, whereas $|\psi(z)|^2$ is in units of $a_\perp^{-1}$.

where $n = 0$ corresponds to the central frustrated site. In Figs. 9(a) and 9(b), we present the occurrences of Anderson-like localization with respect to t for $\beta = 4.5$ and $\beta = 5$, respectively. The occurrences are represented by the condensate fractions at the frustrated lattice sites with time relative to the revival time, $t_R \pm t$. The maximum of each peak signifies a revival of Anderson localization, with the central peak corresponding to t_R. Two important aspects are worth noticing here: (i) The widths of all the peaks are constant for a given β, and this constant width manifests the lifetime of the Anderson localization in any one of the frustrated lattice sites for an initially prepared BOL trap. Figure 9 suggests that the lifetime is greater for larger β [Fig. 9(b)], in spite of having a sharper Anderson localization. (ii) The revival time (distance between two consecutive peak maxima) is different for different β. A larger β or a sharper Anderson localization has a longer revival time. We also calculate the revival times for a tunable BOL (different β) and delineate the variation in Fig. 10 for the localization region ($\beta > \beta_c$). The revival time t_R increases exponentially with β and takes a very high value for a very large β. This signifies a slowing down of tunneling with increasing β and finally reaching a stationary Anderson localization of width $\zeta = c_1 = 0.0048$ [Eq. (20)].

V. DYNAMICAL AND STRUCTURAL STABILITY OF THE ANDERSON-LOCALIZED CONDENSATE

Anderson localization of a BEC happens for a very strong BOL trap, which may hinder the condensate from being stable enough for experimental testing. Hence, we study the numerical stability of the Anderson-localized cloud for their occurrence at $t = 0$ and $t = t_R$. These stability analyses are repeated for various BOL traps with different β and are
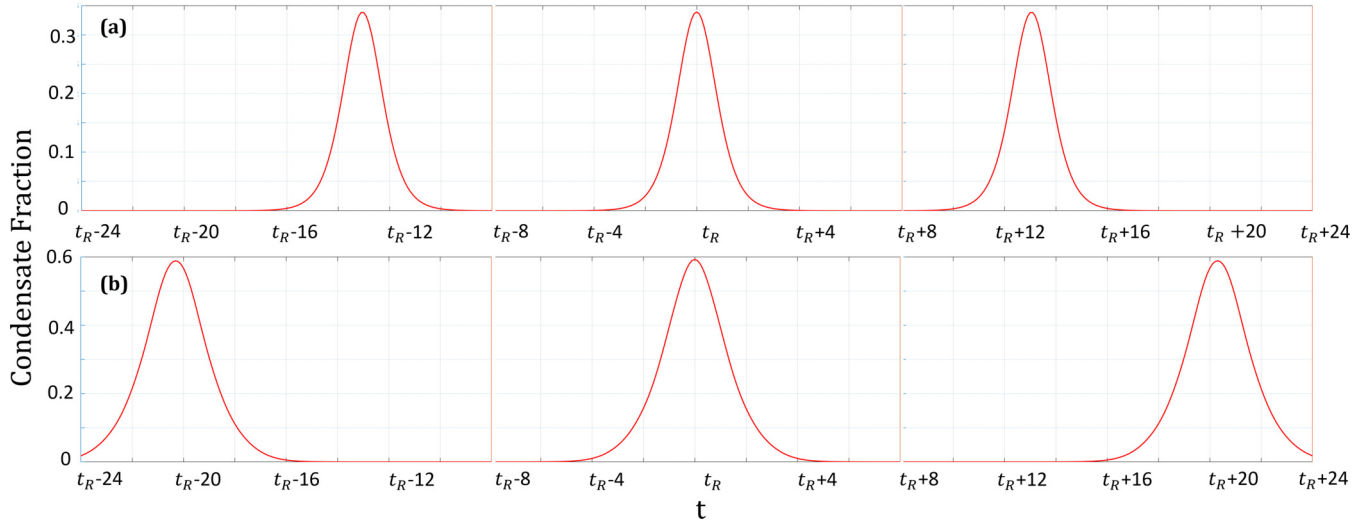
FIG. 9. Occurrence of Anderson localization with time for two β values: (a) 4.5 and (b) 5. They are calculated by evaluating the condensate fraction at the frustrated site. The dimensionless parameters are $G = -1$, $c = 10^4$, $l = 0.84$, $v = 1$, and $\gamma = 0.1$. Here, t is scaled by the inverse of the transverse frequency $\omega_\perp^{-1} = 0.2242$ ms.

depicted in Figs. 11 and 12. We perform a dynamical stability check, where the free evolution of the condensate with and without noise is compared at different times. We executed these analyses by numerically solving the GPE using the split-step Fourier method [31,56–58]. The mean absolute difference of condensate density with noise from that without noise is estimated. We introduced a random noise Δ to our wave function $\psi(z, t)$ at times $t = 0$ and $t = t_R$:

$$\psi_{\text{noise}}(z, t = 0) = \psi(z, t = 0) + \Delta,$$
$$\psi_{\text{noise}}(z, t = t_R) = \psi(z, t = t_R) + \Delta. \tag{21}$$

In Fig. 11, we show the mean absolute difference given by $\text{Mean}[||\psi_{\text{noise}}(z, t)|^2 - |\psi(z, t)|^2|]$ with respect to β, which follows a decreasing trend. We have calculated the mean absolute difference for times $t = 0$ and $t = t_R$, indicated by red dashed and black solid lines, respectively. It is interesting to find that at specific β values, the curves cross each other, thus making them equally stable. The most relevant point we observe is that the mean difference is always below 5% for the localization regime, even with a noise of 10% added to the condensate.

In the case of the structural stability analysis, the evolution of the condensate in the noise-added potential is compared with that in a noiseless potential. Figure 12 shows the mean absolute difference of condensate density in the presence and absence of random noise added to the potential for different β values. The red dashed and black solid lines indicate the mean absolute difference for times $t = 0$ and $t = t_R$. It is worth noting that the mean difference is below 5% even for
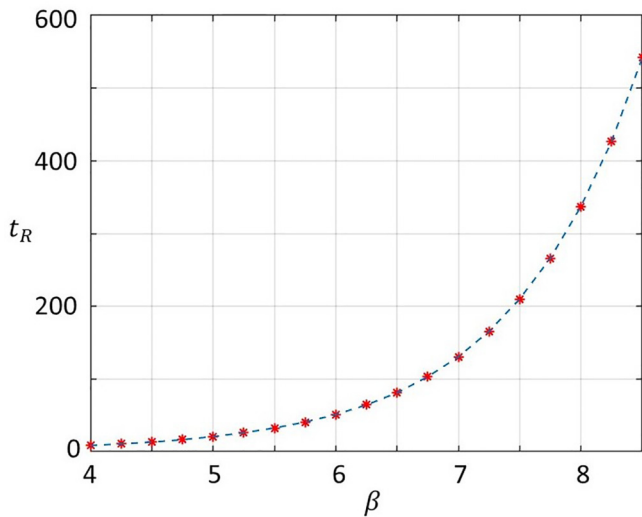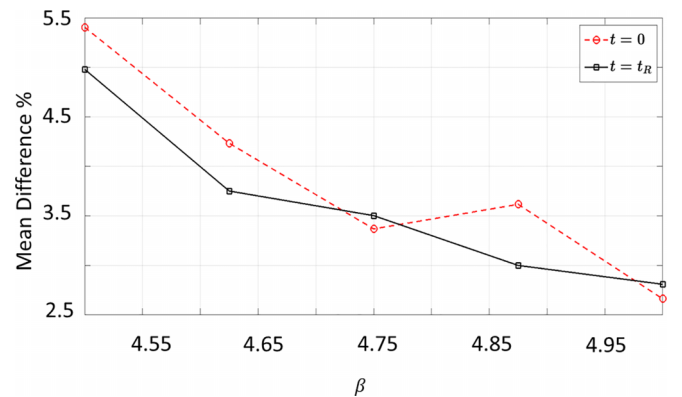

FIG. 10. The variation of revival time t_R of Anderson localization with respect to β. Asterisks show evaluated points. The dimensionless parameters are $G = -1$, $c = 10^4$, $l = 0.84$, $v = 1$, and $\gamma = 0.1$. Here, t is scaled by the inverse of the transverse frequency $\omega_\perp^{-1} = 0.2242$ ms.

FIG. 11. The variation of the mean difference of the condensate density with and without noise with respect to β. The black line indicates the mean difference at $t = t_R$, and the red dashed line indicates the mean difference at $t = 0$.
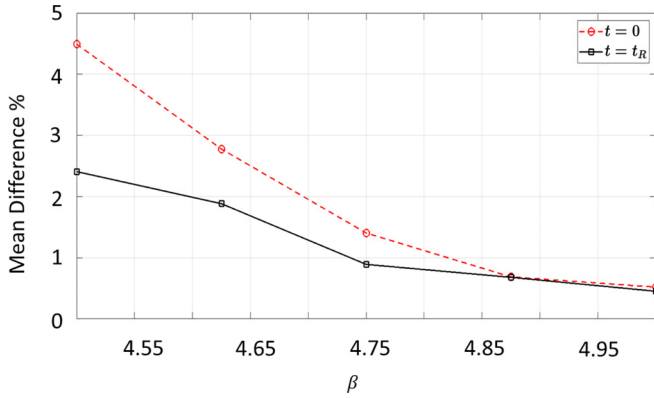
FIG. 12. The variation of the mean difference of the condensate density with and without a noisy potential with respect to β. The black line indicates the maximum difference at $t = t_R$, and the red dashed line indicates the maximum difference at $t = 0$.

the deeper BOL trap ($\beta \geqslant 4.5$) with 10% noise considered in this work. Further, the cloud seems to be more robust to the fluctuations in potential compared to the fluctuations in the wave function. However, in both cases, the mean absolute difference decreases for higher β values corresponding to the localization regime. Hence, the whole analysis presented in this work deals with a very stable Anderson-localized condensate under a BOL.

VI. CONCLUSION

We have presented the time-varying solutions of the 1D GPE for a stationary BOL with a special focus on the dynamics of localized solutions. We have discussed the nature of traveling coordinates and their role in the localization regime. The behavior of localization length and PR with respect to laser power indicates the emergence of strong localization. We proved that the localization that emerges inside the frustrated lattice site varies exponentially and is nothing but Anderson localization. The tunneling of Anderson localization from one site to another is thoroughly understood from the time snapshots of the condensate density. The dynamics of localization in the frustrated site were analyzed separately. The times of occurrence of localization were presented, and the revivals of the Anderson localized cloud were reported. The corresponding revival time was shown to increase with a stronger BOL, implying a slowing down of the tunneling. The dynamical stabilities of the initial time and first revival time were compared, and the values of β for stable localization were reported. This work may be extended for other trap configurations and for a time-varying one.

[1] P. W. Anderson, Absence of diffusion in certain random lattices, Phys. Rev. **109**, 1492 (1958).

[2] P. A. Lee and T. Ramakrishnan, Disordered electronic systems, Rev. Mod. Phys. **57**, 287 (1985).

[3] N. Mott, Conduction in glasses containing transition metal ions, J. Non-Cryst. Solids **1**, 1 (1968).

[4] E. Abrahams, P. W. Anderson, D. C. Licciardello, and T. V. Ramakrishnan, Scaling Theory of Localization: Absence of Quantum Diffusion in Two Dimensions, Phys. Rev. Lett. **42**, 673 (1979).

[5] D. Belitz and T. Kirkpatrick, The Anderson-Mott transition, Rev. Mod. Phys. **66**, 261 (1994).

[6] J. Billy, V. Josse, Z. Zuo, A. Bernard, B. Hambrecht, P. Lugan, D. Clément, L. Sanchez-Palencia, P. Bouyer, and A. Aspect, Direct observation of anderson localization of matter waves in a controlled disorder, Nature (London) **453**, 891 (2008).

[7] G. Roati, C. D'Errico, L. Fallani, M. Fattori, C. Fort, M. Zaccanti, G. Modugno, M. Modugno, and M. Inguscio, Anderson localization of a non-interacting Bose–Einstein condensate, Nature (London) **453**, 895 (2008).

[8] T. Schwartz, G. Bartal, S. Fishman, and M. Segev, Transport and Anderson localization in disordered two-dimensional photonic lattices, Nature (London) **446**, 52 (2007).

[9] G. Modugno, Anderson localization in Bose–Einstein condensates, Rep. Prog. Phys. **73**, 102401 (2010).

[10] L. Fallani, C. Fort, and M. Inguscio, Bose–Einstein condensates in disordered potentials, Adv. At. Mol. Opt. Phys. **56**, 119 (2008).

[11] F. Jendrzejewski, A. Bernard, K. Mueller, P. Cheinet, V. Josse, M. Piraud, L. Pezzé, L. Sanchez-Palencia, A. Aspect, and P. Bouyer, Three-dimensional localization of ultracold atoms in an optical disordered potential, Nat. Phys. **8**, 398 (2012).

[12] M. Sbroscia, K. Viebahn, E. Carter, J.-C. Yu, A. Gaunt, and U. Schneider, Observing Localization in a 2D Quasicrystalline Optical Lattice, Phys. Rev. Lett. **125**, 200604 (2020).

[13] N. Szpak and R. Schützhold, Quantum simulator for the Schwinger effect with atoms in bichromatic optical lattices, Phys. Rev. A **84**, 050101(R) (2011).

[14] A. Long, Tunable bichromatic lattices for ultracold quantum simulation, Ph.D. thesis, University of California, Santa Barbara, 2015.

[15] C. K. Thomas, Quantum simulation of triangular, honeycomb and kagome crystal structures using ultracold atoms in lattices of laser light, Ph.D. thesis, University of California, Berkeley, 2017.

[16] N. Kundu, S. Ghosh, and U. Roy, Quantum simulation of rogue waves in Bose-Einstein condensate: An exact analytical method, Phys. Lett. A **449**, 128335 (2022).

[17] T. Schulte, S. Drenkelforth, J. Kruse, W. Ertmer, J. Arlt, K. Sacha, J. Zakrzewski, and M. Lewenstein, Routes Towards Anderson-Like Localization of Bose-Einstein Condensates in Disordered Optical Lattices, Phys. Rev. Lett. **95**, 170411 (2005).

[18] E. Lucioni, B. Deissler, L. Tanzi, G. Roati, M. Zaccanti, M. Modugno, M. Larcher, F. Dalfovo, M. Inguscio, and G. Modugno, Observation of Subdiffusion in a Disordered Interacting System, Phys. Rev. Lett. **106**, 230403 (2011).

[19] J. Struck, C. Ölschläger, R. Le Targat, P. Soltan-Panahi, A. Eckardt, M. Lewenstein, P. Windpassinger, and K. Sengstock,

Quantum simulation of frustrated classical magnetism in triangular optical lattices, Science **333**, 996 (2011).

[20] S. Nascimbene, Y.-A. Chen, M. Atala, M. Aidelsburger, S. Trotzky, B. Paredes, and I. Bloch, Experimental Realization of Plaquette Resonating Valence-Bond States with Ultracold Atoms in Optical Superlattices, Phys. Rev. Lett. **108**, 205301 (2012).

[21] T. Salger, C. Geckeler, S. Kling, and M. Weitz, Atomic Landau-Zener Tunneling in Fourier-Synthesized Optical Lattices, Phys. Rev. Lett. **99**, 190405 (2007).

[22] D. Poletti, T. J. Alexander, E. A. Ostrovskaya, B. Li, and Y. S. Kivshar, Dynamics of Matter-Wave Solitons in a Ratchet Potential, Phys. Rev. Lett. **101**, 150403 (2008).

[23] J. Bera, A. Q. Batin, S. Ghosh, B. Malomed, and U. Roy, Generation of higher harmonics in dipolar Bose-Einstein condensates trapped in periodically-modulated potentials, Philos. Trans. R. Soc. A (to be published).

[24] M. Modugno, Exponential localization in one-dimensional quasi-periodic optical lattices, New J. Phys. **11**, 033023 (2009).

[25] R. Shiozaki, G. Telles, V. Yukalov, and V. S. Bagnato, Transition to quantum turbulence in finite-size superfluids, Laser Phys. Lett. **8**, 393 (2011).

[26] J. A. Seman, E. A. L. Henn, R. F. Shiozaki, G. Roati, F. J. Poveda-Cuevas, K. M. F. Magalhães, V. I. Yukalov, M. Tsubota, M. Kobayashi, K. Kasamatsu, and V. S. Bagnato, Route to turbulence in a trapped Bose-Einstein condensate, Laser Phys. Lett. **8**, 691 (2011).

[27] O. Dutta, M. Gajda, P. Hauke, M. Lewenstein, D.-S. Lühmann, B. A. Malomed, T. Sowiński, and J. Zakrzewski, Non-standard Hubbard models in optical lattices: A review, Rep. Prog. Phys. **78**, 066001 (2015).

[28] I. A. Bhat, S. Sivaprakasam, and B. A. Malomed, Modulational instability and soliton generation in chiral Bose-Einstein condensates with zero-energy nonlinearity, Phys. Rev. E **103**, 032206 (2021).

[29] S. K. Adhikari and L. Salasnich, Localization of a Bose-Einstein condensate in a bichromatic optical lattice, Phys. Rev. A **80**, 023606 (2009).

[30] A. Nath and U. Roy, Bose–Einstein condensate in a bichromatic optical lattice: An exact analytical model, Laser Phys. Lett. **11**, 115501 (2014).

[31] A. Nath, J. Bera, S. Ghosh, and U. Roy, Exact analytical model for Bose-Einstein condensate at negative temperature, Sci. Rep. **10**, 1 (2020).

[32] S. Schmid, G. Thalhammer, K. Winkler, F. Lang, and J. H. Denschlag, Long distance transport of ultracold atoms using a 1d optical lattice, New J. Phys. **8**, 159 (2006).

[33] M. Sadgrove, M. Horikoshi, T. Sekimura, and K. Nakagawa, Rectified Momentum Transport for a Kicked Bose-Einstein Condensate, Phys. Rev. Lett. **99**, 043002 (2007).

[34] C. Groiseau, A. Gresch, and S. Wimberger, Quantum walks of kicked Bose–Einstein condensates, J. Phys. A **51**, 275301 (2018).

[35] C. J. Pethick and H. Smith, *Bose–Einstein Condensation in Dilute Gases* (Cambridge University Press, Cambridge, 2008).

[36] R. Atre, P. K. Panigrahi, and G. S. Agarwal, Class of solitary wave solutions of the one-dimensional Gross-Pitaevskii equation, Phys. Rev. E **73**, 056611 (2006).

[37] V. N. Serkin and A. Hasegawa, Novel Soliton Solutions of the Nonlinear Schrödinger Equation Model, Phys. Rev. Lett. **85**, 4502 (2000).

[38] Z. X. Liang, Z. D. Zhang, and W. M. Liu, Dynamics of a Bright Soliton in Bose-Einstein Condensates with Time-Dependent Atomic Scattering Length in an Expulsive Parabolic Potential, Phys. Rev. Lett. **94**, 050402 (2005).

[39] Z. Yan and D. Jiang, Matter-wave solutions in Bose-Einstein condensates with harmonic and Gaussian potentials, Phys. Rev. E **85**, 056608 (2012).

[40] J. C. Bronski, L. D. Carr, B. Deconinck, and J. N. Kutz, Bose-Einstein Condensates in Standing Waves: The Cubic Nonlinear Schrödinger Equation with a Periodic Potential, Phys. Rev. Lett. **86**, 1402 (2001).

[41] L. Khaykovich, F. Schreck, G. Ferrari, T. Bourdel, J. Cubizolles, L. D. Carr, Y. Castin, and C. Salomon, Formation of a matter-wave bright soliton, Science **296**, 1290 (2002).

[42] S. Inouye, M. Andrews, J. Stenger, H.-J. Miesner, D. M. Stamper-Kurn, and W. Ketterle, Observation of Feshbach resonances in a Bose–Einstein condensate, Nature (London) **392**, 151 (1998).

[43] T. S. Raju, C. N. Kumar, and P. K. Panigrahi, On exact solitary wave solutions of the nonlinear Schrödinger equation with a source, J. Phys. A **38**, L271 (2005).

[44] S. Burger, K. Bongs, S. Dettmer, W. Ertmer, K. Sengstock, A. Sanpera, G. V. Shlyapnikov, and M. Lewenstein, Dark Solitons in Bose-Einstein Condensates, Phys. Rev. Lett. **83**, 5198 (1999).

[45] K. Strecker, G. Partridge, A. Truscott, and R. G. Hulet, Bright matter wave solitons in Bose–Einstein condensates, New J. Phys. **5**, 73 (2003).

[46] P. A. Ruprecht, M. J. Holland, K. Burnett, and M. Edwards, Time-dependent solution of the nonlinear Schrödinger equation for Bose-condensed trapped neutral atoms, Phys. Rev. A **51**, 4704 (1995).

[47] J. L. Roberts, N. R. Claussen, S. L. Cornish, E. A. Donley, E. A. Cornell, and C. E. Wieman, Controlled Collapse of a Bose-Einstein Condensate, Phys. Rev. Lett. **86**, 4211 (2001).

[48] W. Bao, D. Jaksch, and P. A. Markowich, Numerical solution of the Gross–Pitaevskii equation for Bose–Einstein condensation, J. Comput. Phys. **187**, 318 (2003).

[49] S. L. Cornish, S. T. Thompson, and C. E. Wieman, Formation of Bright Matter-Wave Solitons during the Collapse of Attractive Bose-Einstein Condensates, Phys. Rev. Lett. **96**, 170401 (2006).

[50] A. Gammal, T. Frederico, and L. Tomio, Critical number of atoms for attractive Bose-Einstein condensates with cylindrically symmetrical traps, Phys. Rev. A **64**, 055602 (2001).

[51] A. Gammal, L. Tomio, and T. Frederico, Critical numbers of attractive Bose-Einstein condensed atoms in asymmetric traps, Phys. Rev. A **66**, 043619 (2002).

[52] R. K. Kumar, A. Gammal, and L. Tomio, Mass-imbalanced Bose-Einstein condensed mixtures in rotating perturbed trap, Phys. Lett. A **384**, 126535 (2020).

[53] I. M. Lifshits, S. A. Gredeskul, L. A. Pastur, and E. Yankovsky, *Introduction to the Theory of Disordered Systems* (1988).

[54] S. Mukherjee, A. Spracklen, D. Choudhury, N. Goldman, P. Öhberg, E. Andersson, and R. R. Thomson, Modulation-

assisted tunneling in laser-fabricated photonic Wannier–Stark ladders, New J. Phys. **17**, 115002 (2015).

[55] K. Ishii, Localization of eigenstates and transport phenomena in the one-dimensional disordered system, Prog. Theor. Phys. Suppl. **53**, 77 (1973).

[56] J. Bera, S. Ghosh, L. Salasnich, and U. Roy, Matter-wave fractional revivals in a ring waveguide, Phys. Rev. A **102**, 063323 (2020).

[57] N. Kundu, A. Nath, J. Bera, S. Ghosh, and U. Roy, Synergy between the negative absolute temperature and the external trap for a Bose-Einstein condensate under optical lattices, Phys. Lett. A **427**, 127922 (2022).

[58] B. Halder, S. Ghosh, P. Basu, J. Bera, B. Malomed, and U. Roy, Exact solutions for solitary waves in a Bose-Einstein condensate under the action of a four-color optical lattice, Symmetry **14**, 49 (2021).